



HAL
open science

High-resolution record of tectonic and sedimentary processes in growth strata

Pochat Stéphane, Sébastien Castelltort, Gael Choblet, Jean van den Driessche

► To cite this version:

Pochat Stéphane, Sébastien Castelltort, Gael Choblet, Jean van den Driessche. High-resolution record of tectonic and sedimentary processes in growth strata. *Marine and Petroleum Geology*, 2009, 26 (8), pp.1350-1364. 10.1016/j.marpetgeo.2009.06.001 . insu-00425203

HAL Id: insu-00425203

<https://insu.hal.science/insu-00425203>

Submitted on 12 Apr 2023

HAL is a multi-disciplinary open access archive for the deposit and dissemination of scientific research documents, whether they are published or not. The documents may come from teaching and research institutions in France or abroad, or from public or private research centers.

L'archive ouverte pluridisciplinaire **HAL**, est destinée au dépôt et à la diffusion de documents scientifiques de niveau recherche, publiés ou non, émanant des établissements d'enseignement et de recherche français ou étrangers, des laboratoires publics ou privés.



High-resolution record of tectonic and sedimentary processes in growth strata

Stéphane Pochat^{a,*}, Sébastien Castellort^b, Gaël Choblet^a, Jean Van Den Driessche^c

^a Université de Nantes, LPG Nantes, UMR-CNRS 6112, 2 rue de la Houssinière, BP 92208, 44322 Nantes Cedex 3, France

^b ETH-Zürich, Geological Institute, Sonneggstrasse 5, 8092 Zurich, Switzerland

^c Géosciences – Rennes, CNRS – UMR 6118, Université Rennes 1, Campus de Beaulieu, 35042 Rennes Cedex, France

ARTICLE INFO

Article history:

Received 18 September 2008

Received in revised form

16 April 2009

Accepted 4 June 2009

Available online 13 June 2009

Keywords:

Growth fault

Growth strata

Sedimentary processes

Basin analysis

ABSTRACT

Growth strata are used to determine the kinematics of synsedimentary structures such as faults. Classical methods of analysis such as thickness versus throw plot consider that the available space created by fault slip in the hanging wall of faults is instantaneously filled up by sediments. This has led many previous works to identify a cyclic activity for growth faults. Here we perform a careful analysis of the variation of strata thicknesses on each side of a very well documented normal growth fault in the Niger delta. We show that these thickness variations are induced by the alternation of sedimentary processes during continuous fault slip. Suspended-load processes induce either uniform or slightly variable thickness of a large majority of mudstone layers. Bedload processes result in a preferential thickening of sand layers in the hanging wall. These high quality data thus provide strong grounds for doubting the polycyclic growth diagnosed for some faults at the scale of sedimentary cycles and supports the notion that fault displacement rates can be very well behaved. Our study emphasizes the important conclusion that stable fault growth, and related displacement rates, can appear to be punctuated when viewed at the scale of sedimentary cycles. It follows that care should be taken when attempting to derive displacement rates on temporal scales equivalent to those of alternating sedimentological cycles.

© 2009 Elsevier Ltd. All rights reserved.

1. Introduction

Since growth strata are defined as strata with thickness variations across faults, a synsedimentary fault can be defined as a fault for which incremental displacements have created a fault scarp at the Earth surface. Each incremental displacement of the fault is therefore synchronous with the sedimentary processes of erosion, transport, and sedimentation. Consequently, the degree to which fault evolution induces disturbances of the surface processes is controlled by the ratio between the height of the incremental fault scarp versus the nature and magnitude of the operating sedimentary processes (e.g. volume, thickness, velocity, turbulent/laminar flow, suspended/traction load).

Synsedimentary normal faults (Fig. 1a) originate at crustal scale due to long-term plate movements and at smaller scales in relation with the spreading of a sedimentary cover on a décollement layer (e.g. Edwards, 1976; Price, 1977; Coleman and Prior, 1978; Crans et al., 1980; White et al., 1986; Jackson and White, 1989; Childs et al., 1993; Doglioni et al., 1998; Dawers and Underhill, 2000; Morley et al., 2000; Back et al., 2006).

In the case of gravity-driven tectonics, the long-term behaviour of normal faults over several millions of years is controlled by (1) the evolution of the nature and quantity of the sediment supply and its implications for sedimentary loading and overpressure (e.g. Bruce, 1973; Vendeville and Cobbold, 1988; Ge et al., 1997; Mauduit and Brun, 1998; Gaullier and Vendeville, 2005), (2) the rheology and thickness of the décollement layer (shale versus salt for example) (e.g. Dula, 1991; Childs et al., 1993; Hardy and McClay, 1999; Vendeville, 2005) and (3) the topography of the basement (regional and local slope) (e.g. Crans et al., 1980; Koyi, 1991; Koyi et al., 1993; Mauduit et al., 1997; Loncke et al., 2006).

At higher frequencies of thousands to hundreds of thousand years the interactions between fault evolution and sedimentary process still remains less understood partly because, at these time scales, it is difficult to assess one independently of the other. However, numerous studies have considered that synsedimentary faults can react immediately to sedimentary loading variations. In this view, an increase of sedimentation rate induces an increase of fault displacement, and a decrease of sedimentation rate (i.e. of sedimentary loading) can lead to fault quiescence (e.g. Lowrie, 1986; Cartwright et al., 1998; Bhattacharya and Davies, 2001; Brown et al., 2004).

The main objective of the present work is to deconvolve the very high-resolution temporal and vertical evolution of the throw on

* Corresponding author. Tel: +33 2 51 12 55 86; fax: +33 2 51 12 52 68.
E-mail address: stephane.pochat@univ-nantes.fr (S. Pochat).

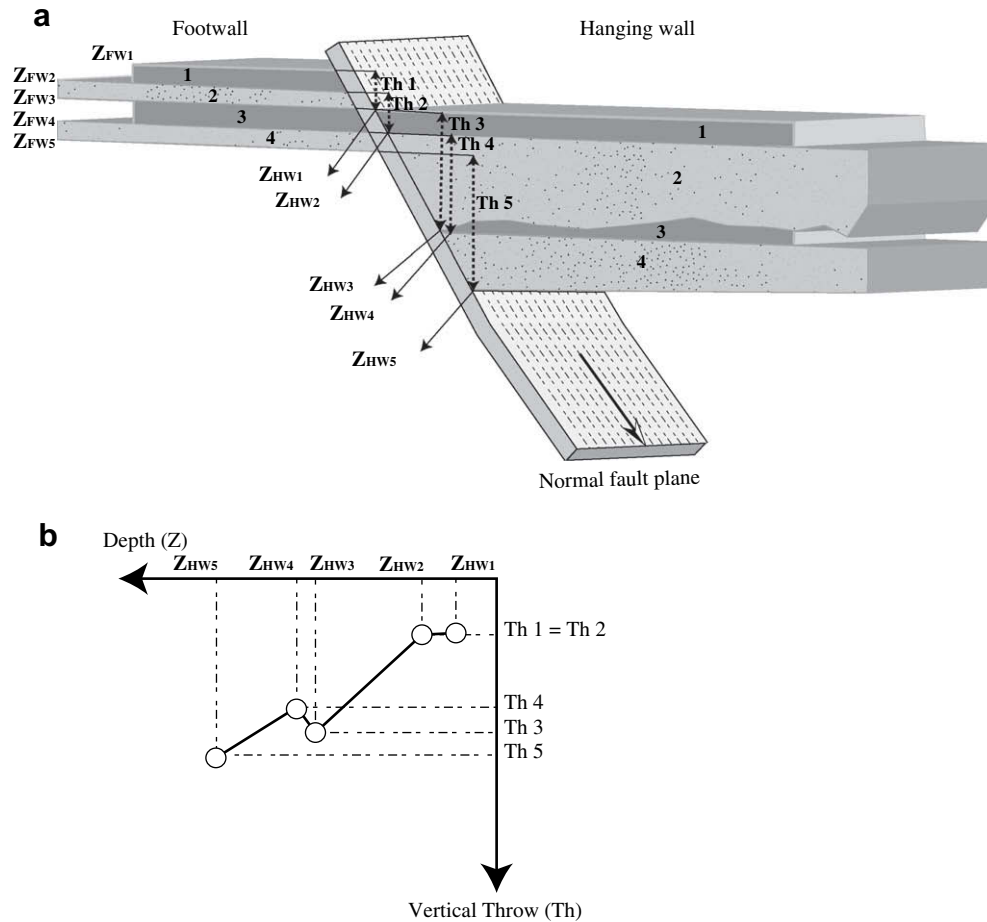


Fig. 1. Signification and construction of a theoretical Th-z plot curve: a) Cross-section of a synsedimentary normal fault with growth strata in the hanging wall. $Z_{HW\ 1-5}$ and $Z_{FW\ 1-5}$ represent the depth of each sedimentary layer limit in the hanging wall and on the footwall respectively. Th1 to Th5 represent the vertical throw of each sedimentary layers limit between the footwall and the hanging wall. b) Vertical throw (Th) versus depth of sedimentary layers in the hanging wall (Z_{HW}) or for the rest of this paper Th-z plot diagram. Note that such a diagram generally shows numerous changes in slope values from positive, null to negative slope which reflects highly variable behaviour in the thicknesses of growth strata between each compartment of the fault.

a well documented normal fault in order to understand the evolution of the long-term to short-term fault movement and the influence of the nature of sedimentary processes (suspended-load, bedload, erosion) on the geometry of the syntectonic layers. We show that high-frequency variations of the growth strata thicknesses across the studied fault are primarily controlled by variations of sedimentary processes and dynamics.

2. Determining fault kinematics from growth strata: an overview

The analysis of the variation of growth strata thickness across a synsedimentary structure allows in principle the reconstruction of its kinematics. For example, the Expansion Index (EI) established by Thorsen (1963) measures the ratio of thickness variation between the layers on the footwall and in the hanging wall of a synsedimentary normal fault (Fig. 1a):

$$EI = \frac{HWt}{FWt} \quad (1)$$

with HWt and FWt corresponding to the thickness of the layers in the hanging wall and the footwall respectively. $EI > 1$ represents a thickening in the hanging wall. Thus, assuming that sedimentation rate is constant over the footwall, positive and variable values

of EI (i.e. increase or decrease of HWt relative to FWt) can be directly related to variations of the fault movement rate (Hardin and Hardin, 1961; Thorsen, 1963).

The Th-z plot (Fig. 1a, b) is a graphical method which simply consists in plotting, for each horizon, the vertical throw Th of a stratigraphic marker versus its depth z in the hanging wall (Tearpock and Bischke, 1991; Bischke, 1994) (Fig. 1a, b). This kind of plot generally shows alternation of segments of positive, null and negative slopes which directly reflect variations in the degree of thickening of the strata towards the hanging wall (Bischke, 1994; Mansfield and Cartwright, 1996; Cartwright et al., 1998; Castellort et al., 2004a, b; Pochat et al., 2004; Back et al., 2006; Baudon and Cartwright, 2008) (Fig. 1b).

If the sedimentation rate in the hanging wall always exceeds the fault displacement rate ("fill-to-the-top" model) the Th-z plot can be used to constrain the displacement history of synsedimentary faults (Tearpock and Bischke, 1991; Bischke, 1994; Mansfield and Cartwright, 1996; Cartwright et al., 1998). Thickening of strata towards the hanging wall indicates a period of fault activity (positive slopes, between Z5-Z4 and Z3-Z2 in Fig. 1b), non-thickened intervals indicate periods of fault quiescence (null slopes, between Z2 and Z1 in Fig. 1b), and negative slopes (between Z4 and Z3 in Fig. 1b) may indicate fault linkage (Tearpock and Bischke, 1991; Bischke, 1994; Mansfield and Cartwright, 1996; Cartwright et al., 1998) or fault inversion (Castellort et al., 2004b). Castellort

et al. (2004b) demonstrated that the slope α_i in a Th–z plot, in the “fill-to-the-top” model, is another expression of EI (Thorsen, 1963)

with $\alpha_i = 1 - EI^{-1}$. (2)

In this way, $\alpha_i = 0$ corresponds to $EI = 1$, $\alpha_i > 0$ corresponds to $EI > 1$ and $\alpha_i < 0$ corresponds to $EI < 1$. The additional information displayed by Th–z plots which lacks in the Expansion Index method (Thorsen, 1963) is the absolute magnitude of vertical displacement on the considered fault.

This type of analysis has been extended at larger scales and completed with additional absolute or relative dating in several studies. Some of these studies use expansion or growth index (e.g. Gibbs, 1983; Beach, 1984) which compound fault and sedimentation rates i.e. they are dependent both on potential changes in the fault displacement rate and on changes in sedimentary processes and in stratigraphic cycles. Others studies (e.g. Nicol et al., 1997, 2005; Meyer et al., 2002; Walsh et al., 2002; Mouslopoulou et al., 2009) look at displacement versus age (or time) at temporal scale greater than high-frequencies stratigraphic cycles and sedimentary processes i.e. regardless of sedimentation processes and stratigraphic cycle. At such scale of observation, the fault displacement is found to be relatively stable at scale ranging from less than 100 kyr up to several tens of millions of years.

Those studies are based on the principle that at the time scale of observation (1) the sedimentation rate in the hanging wall always exceeds the fault displacement with a minimum factor of 1/30, and (2) the erosion on the footwall is not significant.

More generally, it is usually assumed that:

- (1) thickness variations are directly the result of variations of fault displacement rate;
- (2) at the scale of the analysis, the creation and existence of incremental fault scarps are always negligible.

With respect to the first assumption, Bischke (1994) initially noted that the Th–z plot analysis could also provide information about the contemporaneous sedimentary process. For example Bischke (1994) observed that (1) a negative slope often correspond to a condensed deposit in the hanging wall (e.g. as between Z4 and Z3 in Fig. 1b) and (2) any change in the sedimentation may create a slope break in Th–z plot. These basic observations remind us simply that the thickness of syntectonic deposits contains always two superimposed pieces of information: (1) one about the fault movement which creates the available sedimentary space and (2) the other about the sedimentary processes (rate and dynamics). The interpretation of syntectonic thickness variations is thus unlikely to be unequivocal.

With respect to the second assumption, synsedimentary fault scarps have been widely documented on the present-day sea floor and in ancient deposits through their influence on sedimentary processes in a range of depositional settings (e.g. Petit and Beauchamp, 1986; Thornburg et al., 1990; Leeder and Jackson, 1993; Edwards, 1995; Morris et al., 1998; Newell, 2000; Hodgetts et al., 2001; Hodgson and Haughton, 2004; Pochat and Van Den Driesche, 2007). On the present-day sea floor, Ocamb (1961) and Oakes (1959) document fault scarps on which undergo no deposition or even erosion, whereas the subsiding compartments of the faults they study is a zone of strong deposition. In this case thickness variation on both sides of a fault has no straightforward relation with the magnitude of the displacement. In such a case, the assumption of “fill-to-the-top” sedimentation, which is required to interpret growth strata in terms of fault kinematics, is not always justified (Childs et al., 2003; Castelltort et al., 2004a, b; Pochat et al., 2004).

In most depositional settings (deltaic, deep-water, fluvial) sedimentation is always made up of stratigraphic cycles characterized primarily by the alternation of fine suspended-load deposit (settling out of suspension load) and coarser bedload deposit which produce typical sand-shale alternations (Damuth, 1994; Edwards, 1995; Cross and Lessenger, 1998; Soreghan et al., 1999; Hiscott, 2001). The different processes record in different ways the differential subsidence due to growth faulting. Settling out of shale particles (decantation) produces sedimentary layers homogeneously distributed across faults (Lowrie, 1986; Cartwright et al., 1998; Hiscott, 2001), without being diffused to topographic lows on time scales of 10–100s ka (Mitchell, 1996; Webb and Jordan, 2001). In contrast, bedload deposition of sands tends to fill the topographic lows before the highs.

Castelltort et al. (2004b) have proposed that, if fault displacement is treated as a continuous process on the scale of depositional cycles, the slope variations on a Th–z plot may be interpreted as fault-induced topography variations which can be in turn directly related to changes of the sedimentary dynamics, as in the case of alternating sand and shale deposition. In their work, were presented the interpretation of a Th–z plots with the two end-members “fill-to-the-top” model (Fig. 2a) and “variable displacement/topography” or “fault scarp” model (Fig. 2b) (Castelltort et al., 2004b).

In the first model (Fig. 2a), all the slope variations are controlled by a combination of fault displacement rate and sedimentation rate. With a constant displacement rate any change in the sedimentation rate will produce a change in slope segment in the Th–z plot diagram. For example, a large increase of the sedimentation rate will produce a diminution of slope. A zero slope on the Th–z plot indicates a cessation of the fault movement.

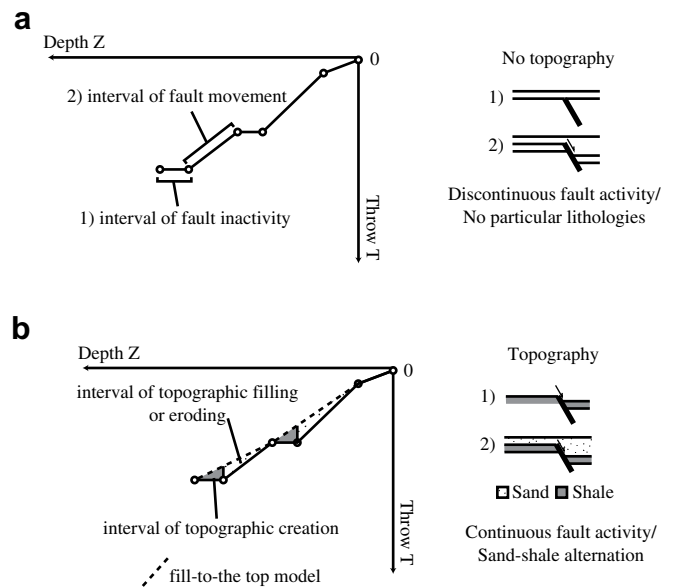


Fig. 2. Significance of Th–Z plot slope variation (Castelltort et al., 2004a, b). a) “Fill-to-the-top” model: Each slope variation characterizes the ratio between fault displacement rate and sedimentation rate. A zero-slope interval is symptomatic of fault inactivity. A positive-slope interval is symptomatic of fault activity. b) “Fault scarp” model: Alternation of zero-slope segments and positive-slope segments corresponds to alternation between topographic creation and topographic filling (or eroding) intervals. Each pair of topographic creation and filling-eroding intervals defined on the Th–Z plot makes it possible to trace a lower curve envelop (dashed line) that corresponds to a “fill-to-the-top” model in this interval. On each portion of this curve the ratio between fault displacement and the sedimentation rate is assumed to be constant. However, every slope variation between each portion of the curve is considered to be representative of the variation in this ratio.

In the second model (Fig. 2b), the slope variations are a consequence of alternative period of fault scarp creation and fault scarp filling or eroding. Preservation of fault scarp on the sea floor is more likely associated with sedimentary processes such as suspended-load deposit which prevent rapid smoothing of the topography. Fault scarp filling is preferentially associated with “dynamic” bedload processes. With this perspective, slope variations on the Th–z plot can be directly linked to lithological variations, and null slopes can be associated with dominant shale/mud layers rather than sand layers.

In absence of a permanent lithological control on both sides of a fault, the Th–z plot method may introduce a bias in the analysis of fault kinematics because alternating between null slopes and positive slopes can be interpreted as the result of two opposite end-member processes (Lowrie, 1986; Cartwright et al., 1998; Castellort et al., 2004a, b; Pochat et al., 2004): either (1) the alternation of periods of suspended-load deposit (settling out of suspension load) and bedload deposit (favouring alternating fault scarp preservation and filling) over a continuous fault movement, or (2) the alternation between periods of fault inactivity and activity over a constant sedimentation rate background.

3. Geological setting

The Niger delta develops within the Gulf of Guinea on a surface of about 140 000 km² (Fig. 3) for a sediment thickness of about 12 km. This siliciclastic system began to prograde across the pre-existing continental slope into the deep sea during the Late Eocene (Burke, 1972) and is still active today. The stratigraphy of the Niger delta can be divided into three major transgressive units of Paleocene, Oligocene and recent ages respectively (Short and Stauble, 1967). The lowermost formation of Akata includes 6500 m of marine clays with silty and sandy interbeds (Whiteman, 1982). The intermediate formation of Agbada is characterized by paralic to marine deltaic deposits mainly composed of sandstones and shales. The uppermost unit, the Benin formation comprises fluvial sands, gravel and back swamp deposits (2500 m thick).

The continental margin off the Niger Delta is undergoing deformation caused by the seaward movement of the underlying overpressured shale (Akata formation) which acts as a mobile substrate, similar to natural evaporites deforming in response to deltaic progradation and sedimentary loading (e.g. Merki, 1972; Doust, 1990; Doust and Omatsola, 1990; Cohen and McClay, 1996a, b). Consequently in the delta top, the sedimentation was concentrated in numerous arcuate depobelts bounded by large-scale regional and counter-regional growth faults (Doust, 1990; Doust and Omatsola, 1990) (Fig. 3). The activity of each depobelt progresses in time and space towards the SSW in relation to the alluvial progradation facilitated by large-scale withdrawal and forward movement of the underlying shale (Damuth, 1994; Cohen and McClay, 1996a). The outer shelf and the upper slope of the Niger Delta are characterized by the evolution from an extensional zone to a translational zone of diapir and shale ridges which evolved eventually into a compressional zone of imbricate toe thrusts beneath the lower slope and rise (Vannier and Durand, 1994; Schulbaum et al., 1996).

Our study is located in the upper part of the modern Niger delta, in the southeastern part of the Greater Ughelli Belt, 90 km north of Port-Harcourt (Fig. 3) and was carried out on an NW–SE normal fault which intersects the Agbada formation (Fig. 4a, b). This fault is sealed under 2000 m of sedimentary deposits which indicated that its period of activity was restricted during the deposition Agbada formation. We used sets of lithological data, provided by Total, on 2 wells (Pochat et al., 2004) that are positioned on either side of the fault and almost perpendicular to the fault direction (Fig. 4a, b). The fault affected four major depositional environments which have been recognized in this formation (Vannier and Durand, 1994; Schulbaum et al., 1996): (1) upper deltaic plain, (2) tidal zone, (3) delta front and (4) pro-delta shales. In the study area, the delta mainly prograded southward during Early Oligocene to Late Miocene times. In this dataset, 10 major maximum flooding surfaces (mfs, Table 1) record the most argillaceous intervals and define 9 major stratigraphic cycles (Regressive–Transgressive cycles) (Pochat et al., 2004). The vertical position and relative age of

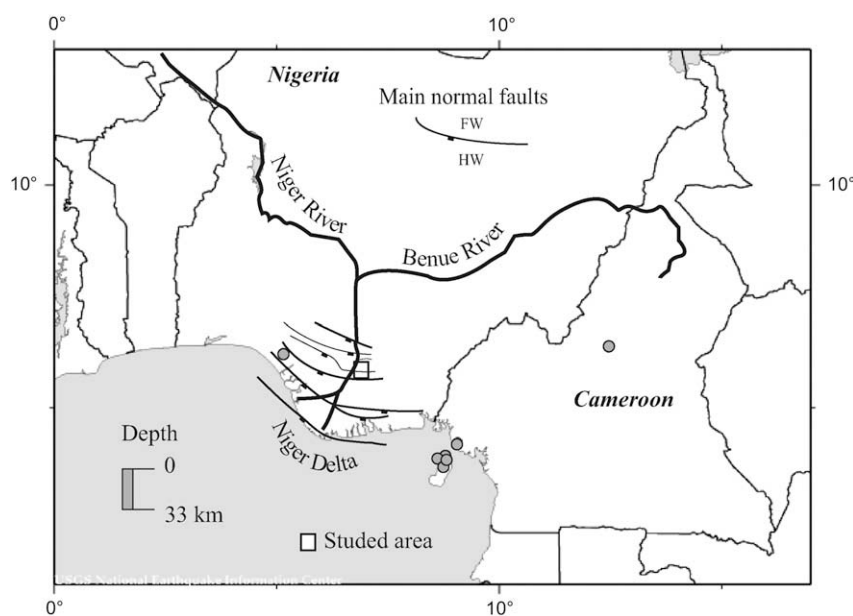


Fig. 3. Regional map of the continental part of the Niger delta. The studied area (rectangle) is located on the Greater Ughelli depobelt region (Doust and Omatsola, 1990). The map also shows the seismic activity (USGS/NEIC Earthquake Catalog 2007) of the West African region including the Niger delta region. Note that only 10 earthquakes with magnitude > M4 have been recorded in this part of Africa between 1974 and 2000 and only one in the Niger delta whereas the faults are still active today (e.g. Adeogba et al., 2005; Damuth, 1994; Heinio and Davies, 2007; Hooper et al., 2002; Magbagbeola and Willis, 2007; Owoyemi and Willis, 2006).

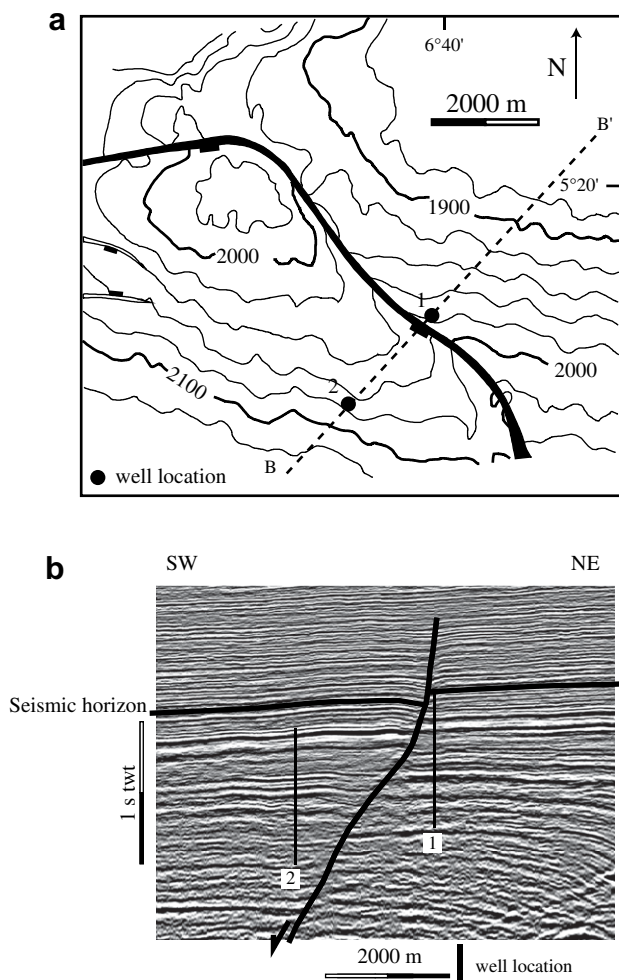


Fig. 4. Presentation of the studied area. a) Map of studied fault (black fill) for horizon indicated on b, depth is in ms TWT. The studied normal fault is oriented NW–SE and shows a relatively arched profile. The location of the cross-section is shown by the dashed line B–B' in Fig. 5. The location of wells is indicated by the black circles. b) Seismic SW–NE cross-section showing NW–SE normal fault. Location of the wells is indicated by the black vertical lines. Note that the vertical throw seems to decrease gradually and eventually is tend to be equal to zero (embedded fault) from the bottom to the top of the fault.

each mfs were provided by Total (Pochat, 2003) and correlated with the Mesozoic–Cenozoic sequence-chronostratigraphic chart (Hardenbol et al., 1998) which gives ages comprised between 29 and 18 My, and a duration of 0.5–3 My for individual cycles

Table 1

Maximum flooding surface age (in My) and vertical throw (in m). The relative age with error bar of each maximum flooding surface are deduced from comparison from Mesozoic–Cenozoic sequence-chronostratigraphic chart (Berggren et al., 1995; Hardenbol et al., 1998) and data provided by Total (Pochat, 2003). In bold, the age of mfs 3d and mfs 4c were obtain with biostratigraphic constraint (Pochat, 2003). The vertical throw are extracted from well log data (This study).

	Age (My)	Error (My)	Throw (m)
mfs 3d	18.2	0.3	15
mfs 3c	21.2	0.3	50
mfs 4e	22.6	0.6	135
mfs 4d	23.3	0.3	230
mfs 4c	23.9	0.3	290
mfs 4b	24.9	0.3	420
mfs 4a	25.9	0.3	520
mfs 5c	27	0.3	620
mfs 5b	28.3	0.3	750
mfs 5a	29.2	0.2	830

(Table 1), the age of mfs 3d and mfs 4c were obtain with biostratigraphic constraint (Pochat, 2003). The maximum error estimated on the age of the different mfs evolved from 0.2 to 0.6 My (Table 1) (Pochat et al., 2004).

4. Method of decompaction

In order to compute the decompacted thicknesses of the various sediment layers, we have adapted a simple procedure from Sclater and Christie (1980) with local petrophysical values adapted to Niger delta settings from Chukwueke et al. (1992). The decompaction method is a meter-per-meter sequential decompaction of footwall and hanging-wall sequences and computation of fault throw with the same approach and mathematical formalism used by Taylor et al. (2008) (see Appendix A for further details). The throw decompaction method would principally have the effect of increasing fault throws but would not alter the shorter time scale variability in displacement rates (Taylor et al., 2008) which is at the heart of this study. The borehole data provided by Total (Pochat, 2003) has a threshold resolution of 1 m. The routine used to decompact gives results of thickness with decimal which have no significance. Thus, in this study, no change in throw or thickness variation less than 1 m has been taken into account.

5. Lithological column description

The deposits are constituted of 26 sandstone layers and 25 mudstone layers, for a total thickness in the hanging wall of 3670 m (Fig. 5). In the hanging wall, 8 sedimentary layers are found that have no equivalent on the footwall, of which 6 are mudstone layers included in thicker sandstone layers (S8–S10–S11–S12–S13–S15) and 2 are sandstone layers included in thicker mudstone layers (A7) (Fig. 5). On the footwall there are 2 extra layers made of mud included in sandstone layers (S24–S25) (Fig. 5). The mud-rich deposits are made up of 3 layers of offshore clays deposited above the storm wave base which constitute the deeper facies present here (basal part of A7, below mfs 4c, A11–A13) (Fig. 5). Two sandstone layers have strong erosive bases and tops (S16–S24) (Fig. 5) which are both considered as regional erosive events (Pochat, 2003).

6. Throw versus times analysis

In order to determine the predominant factor that controls short-term thickness variations in growth strata, i.e. fault movement or sedimentation dynamics, we first analysed the long-term evolution of the fault displacement rate during time.

Our analysis focuses on the variation of the vertical throw of each mfs during time (Fig. 6). The benefit of using these particular stratigraphic surfaces is that they can be considered as representing a nearly instantaneous event at the scale of a sedimentary basin or such kilometeric structures (Van Wagoner et al., 1988; Mitchum and Van Wagoner, 1991). Mfs are also not usually associated with erosive events which may preclude the interpretation of the true fault displacement (Childs et al., 1993). Thus, we assume that the measured vertical throw of each mfs (between the footwall and the hanging wall) is the closest approximation of the true fault displacement, i.e. corresponds to the case of no fault scarps. This analysis corresponds to the “fill-to-the-top” model (Castelltort et al., 2004a, b). In order to minimize at best the error on the vertical throw estimation and the relative ages of each mfs, we have estimated the displacement rate from the best appropriate fitting on the entire curve (Fig. 6).

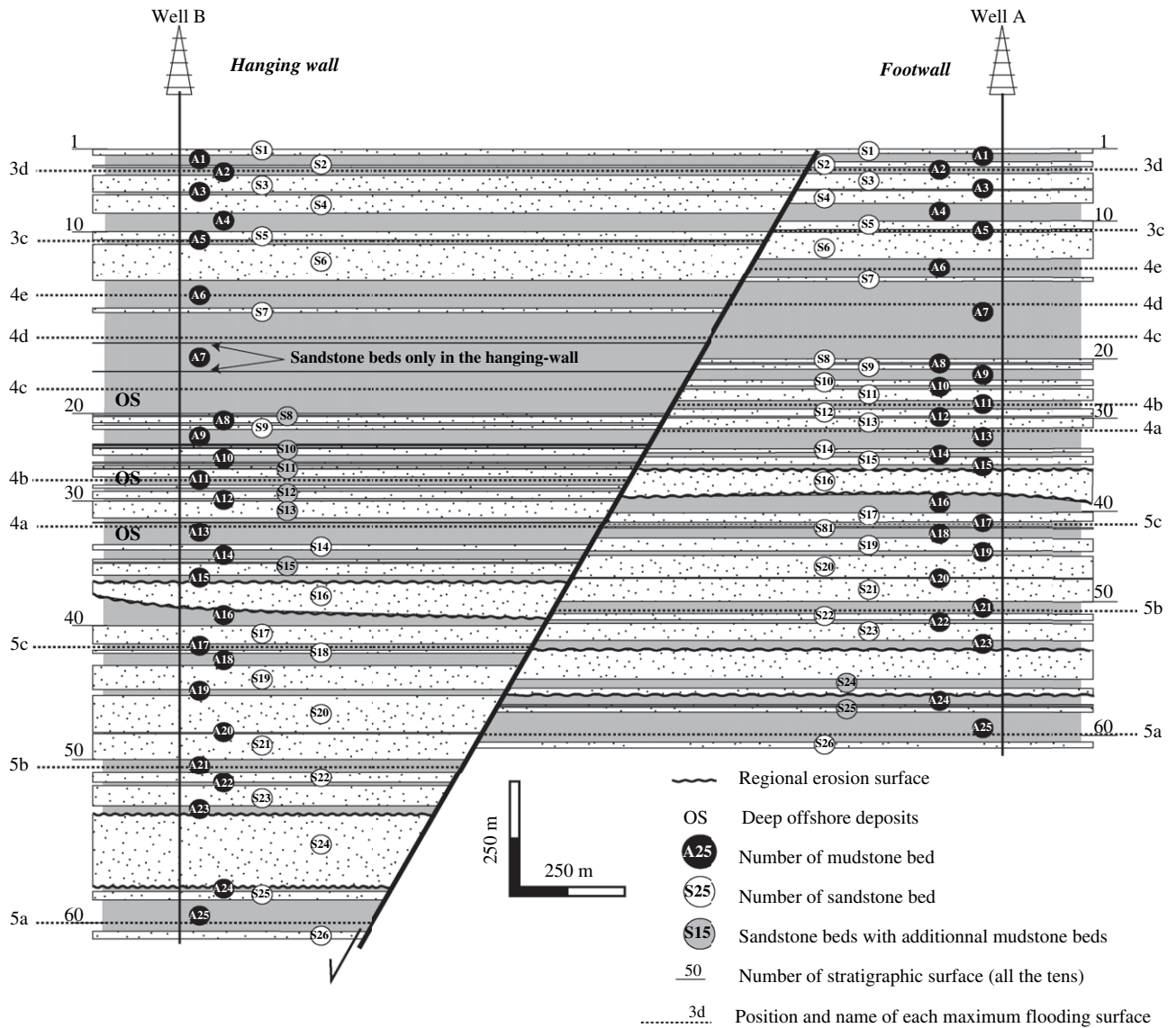


Fig. 5. Restored cross-section of the normal fault and associated lithological column extracted from well log data (Well A and B) provided by Total (Pochat, 2003). Mudstone layers are represented with grey colour and number of each layers are in black circle, sandstone layers are represented with small points and number of each layers are in white circle and grey circle. Each grey circle indicated the presence of extra mudstone layers in sandstone layers. Extra sand layers are only present in the thicker mudstone layer 7. The regional erosion surface is represented by black wavy lines. The abbreviation OS indicates purely Offshore Shale deposited under the storm wave base (Pochat, 2003). The position of each maximum flooding surface (3d, 3c, 4e, 4d; 4c, 4b, 4a, 5c, 5b, 5a) is indicated by horizontal dotted line on each compartment of the fault. The number of stratigraphic surfaces (sandstone/mudstone transition and mfs position) is 62 and are re only numbered all the tens. The thickness of the lithological column is represented in its initial state that is to say undecompressed.

The analysis shows that the vertical throw encompasses a long-term, progressive diminution with time from 830 m to 15 m, over 10 millions of years (Fig. 6). This evolution occurs without any short-term break in slope which implies a continuous fault displacement during 10 million year. Also, the fact that the youngest marker has horizontally sealed the fault (Fig. 6), suggests a long-term dampening of the fault displacement rate with time. Indeed, the fault movement can be divided into 2 phases (Fig. 6): a first longer phase from -29.5 to -21.5 My (8 My) with a rate of displacement of 90 to 120 m/My (0.09–0.12 mm/y) abruptly followed by a second, shorter phase from -21.5 My to -18 My (3.5 My) with a rate of displacement of 10 to 15 m/My (0.01–0.015 mm/y). Since a straight line can be fitted to all but the final and most recent point on the curve (mfs 3d), we considered that fault growth rates were constant for 800 m of the total 850 m

throw history (i.e. ca 95%) during 10 My (Fig. 6). The unusual or shifted position of mfs 3d may be the expression of a brutal shutting down of the growth fault during this period. This brutal cessation of activity could be correlate to the sealed character of the fault inside the Agbada formation (Fig. 4a,b). However, we cannot ruled out that the low value of mfs 3d vertical throw (10 m throw) may be attributed to compaction-related displacement losses which are more significant at low displacements (Taylor et al., 2008). In this case, it is possible to envisage that the fault displacement was constant until just before mfs 3d times (i.e. for nearly 98% of the growth history).

Such long-term continuous rate of fault displacement over such time scales has been previously described in different tectonic and sedimentary settings (Nicol et al., 1997, 2005; Walsh et al., 2002; Childs et al., 2003) and is characteristic of long-term behaviour of

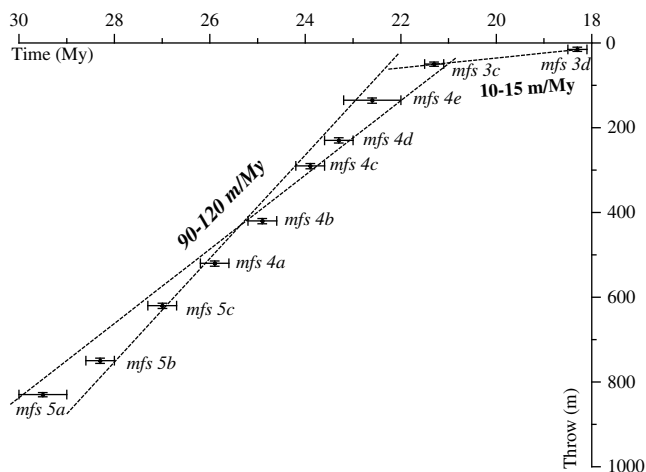


Fig. 6. Evolution of the vertical throw of each maximum flooding surface during time. The borehole data provided by Total (Pochat, 2003) has a threshold resolution of 1 m. The routine used to decompact give results of thickness with decimal which have no significance. Thus, in this study, no change in throw or thickness variation less than 1 m has been taken into account. Absolute age and error bars for each mfs are given Table 1.

synsedimentary faults in a context of gravity-driven tectonics (Ocamb, 1961). The highest displacement rates (0.1–0.12 mm/y) are equivalent to moderate displacement rates for fossilized normal faults in similar tectonic settings (Nicol et al., 1997, 2005), and to present-day normal faults in the Mississippi river delta i.e. 0.1–1 mm/y (Gagliano et al., 2003). For the latter, Gagliano et al. (2003) indicates that, since 1960, the Louisiana is affected by active extensional faulting associated with normal fault scarps of 0.3–1.1 m high over 5–8 km lengths. We note that these high rates of fault movement are not associated with a significant seismic activity (USGS/NEIC Earthquake Catalog 2007). Similar active normal faults in the present-day Niger delta show the same

behaviour, i.e. the creation of fault scarps without seismic rupture (Fig. 3). Aseismic behaviour of faults is found when deformation occurs by “creeping” along the fault plane. Such behaviour is favoured when faults merge at depth with décollement layers, such as the shale-rich Akata formation in the Niger Delta (Merki, 1972; Doust, 1990; Doust and Omatsola, 1990; Cohen and McClay, 1996a, b). The ductile behaviour of shales strongly depends on fluid pressure and can vary with time and space (Morley and Guerin, 1996). Our observation of long-term continuous fault displacement rate during 10 million years suggests that the ductile behaviour of the Akata shale layer remained stable at this time scale.

We can therefore assume a continuous fault displacement over time scales of hundreds of thousand years (average duration of P–R cycles) to several millions of years.

7. Throw versus depth analysis using Th–z plots

The first feature observed on the Th–z plot is the long-term quasi linear decrease of the vertical throw from 835 to 0 m, over a sediment thickness of 3670 m (Fig. 7). At higher resolution we note that the Th–z curve is characterized by short-term variations in slope between each point of the curve (Fig. 7).

Because the mfs are clearly defined stratigraphic surfaces on either sides of the fault, we have added theirs positions (compare Figs. 7 and 8). The objectives are (1) to increase precision of the Th–z plot and (2) to subdivide a number of thick mud deposits. For example without mfs position, the thicker mudstone layer (A7) has only 2 points of measure over a thickness of 500 m (Fig. 7).

In order to more precisely define the values and origin of the observed slope variations on the Th–z curve we report the slope variation values versus the hanging-wall thickness evolution (Fig. 8) for each sandstone layer (S1–S26) and mudstone layer (A1–A25). We also report the position of each mfs inside their associated mudstone layers (mfs 5a in A25, mfs 5b in A21, mfs 5c in A17, mfs 4a in A13, mfs 4b in A11, mfs 4c and mfs 4d in A7; mfs 4e in A6, mfs 3c in A5, mfs 3d in A2, see Fig. 5).

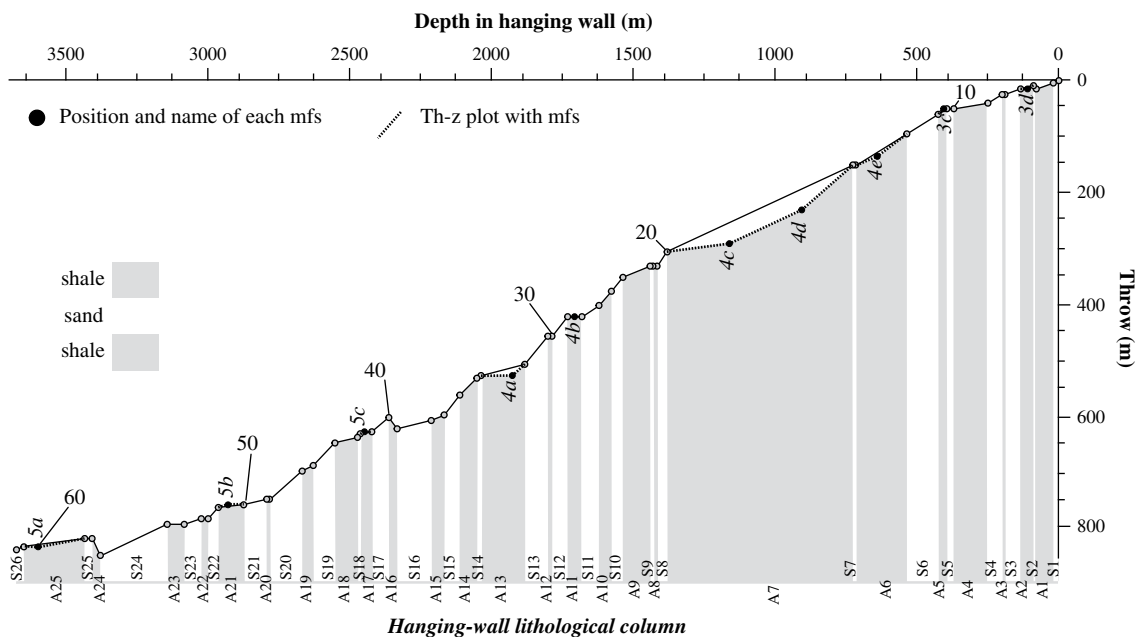


Fig. 7. Th–z plot curve correspond to the vertical throw (y-axis) plotted against the cumulative thickness or depth (x-axis) of sediment in the hanging wall. We have added (1) the position and name of each maximum flooding surface and associated Th–z plot curve and (2) the all tens numbers of stratigraphic surface. We have also added a simple description of the hanging-wall lithological column, with grey fill corresponding to mudstone layers with name of each layer from A1 to A25 (left to right) and white fill corresponding to sandstone layers with name of each layer from S1 to S26 (left to right).

The introduction of the mfs has no effect on the slopes for mfs 5c–4b i.e. no change of vertical throw on the curve (Figs. 7 and 8). We note minor effects for mfs 5a, 5b, 4e, 3c and 3d (Fig. 8) i.e. 5–10 m below the initial curve (Fig. 7) and major effects for mfs 4c, 4d, and 4a (Fig. 8), i.e. 35–40 m below the initial curve (Fig. 7).

In the Th–z plot, a zero-slope interval corresponds to an unthickened layer on both sides of the fault, a positive slope corresponds to a thicker deposit in the hanging wall and a negative slope corresponds to a thinner deposit in the hanging wall (thicker deposit on the footwall (Castelltort et al., 2004a, b; Pochat and Van Den Driessche, 2007) (Fig. 8).

The major striking feature of this Th–z plot (Figs. 7 and 8) is that 22 sand-to-shale transitions over 24 (i.e. 90%) are associated with short-term changes of the slope on the Th–z curve (excepted between A5–S5 and A8–S9).

Thus, in term of slope variation, we have distinguished 4 major tendencies (Fig. 8):

- (1) 13 layers show an equal thickness on both sides of the fault (i.e. zero-slope segment, S5–S7–S9–S25 and A3–A4–A8–A11–A12–A17–A20–A21–A22–A23). Considering additional mudstone layers with mfs subdividing adds 4 new unthickened mudstone layers in A2–A5–A13–A25. This gives a total of 17 unthickened deposits. Nine unthickened deposits over 13 (70%) i.e. without

mfs subdividing, or 13 unthickened deposits over 17 (75%) with additional mfs subdividing, are made of shale.

- (2) Three layers are thinned in the hanging wall (negative slope, A24, A16 and S2), of which 2 are made of shale.
- (3) 35 layers over 51 (i.e. 70% of the layers) are thicker in the hanging wall which confirm the syndimentary nature of the normal fault. Among these 35 thickened layers (or among the 39 with mfs subdividing (Fig. 8), 21 are made of sand (i.e. 60% and 55% respectively).
- (4) 18 over 25 of the mudstone layers (70%) are systematically thinner than their immediate overlying sandstone layers, i.e. the sandstone layers are systematically thicker in the hanging wall than their immediate underlying mudstone layers. Thus 10 layers (11 layers with mfs in A5) show slope variations greater than 0.5 (i.e. 200% of thickness variation) of which 8 are sandstone layers (75–80%) and 2 are mudstone layers (+1 layer within A5); 12 layers (15 layers with mfs in A5–A7–A13) show slope variations greater than 0.4 (i.e. 170% of thickness variation) of which 10 are sand layers (65–80%) and 2 are mudstone layers (+3 layers with mfs in A5–A7–A13) and 6 layers show slope variation greater than 0.6 (i.e. 250% of thickness variation) which all are made of sand.

The largest differential of thickness variation is between the layer A24 and S8, with a value of 700% of variation, the most important

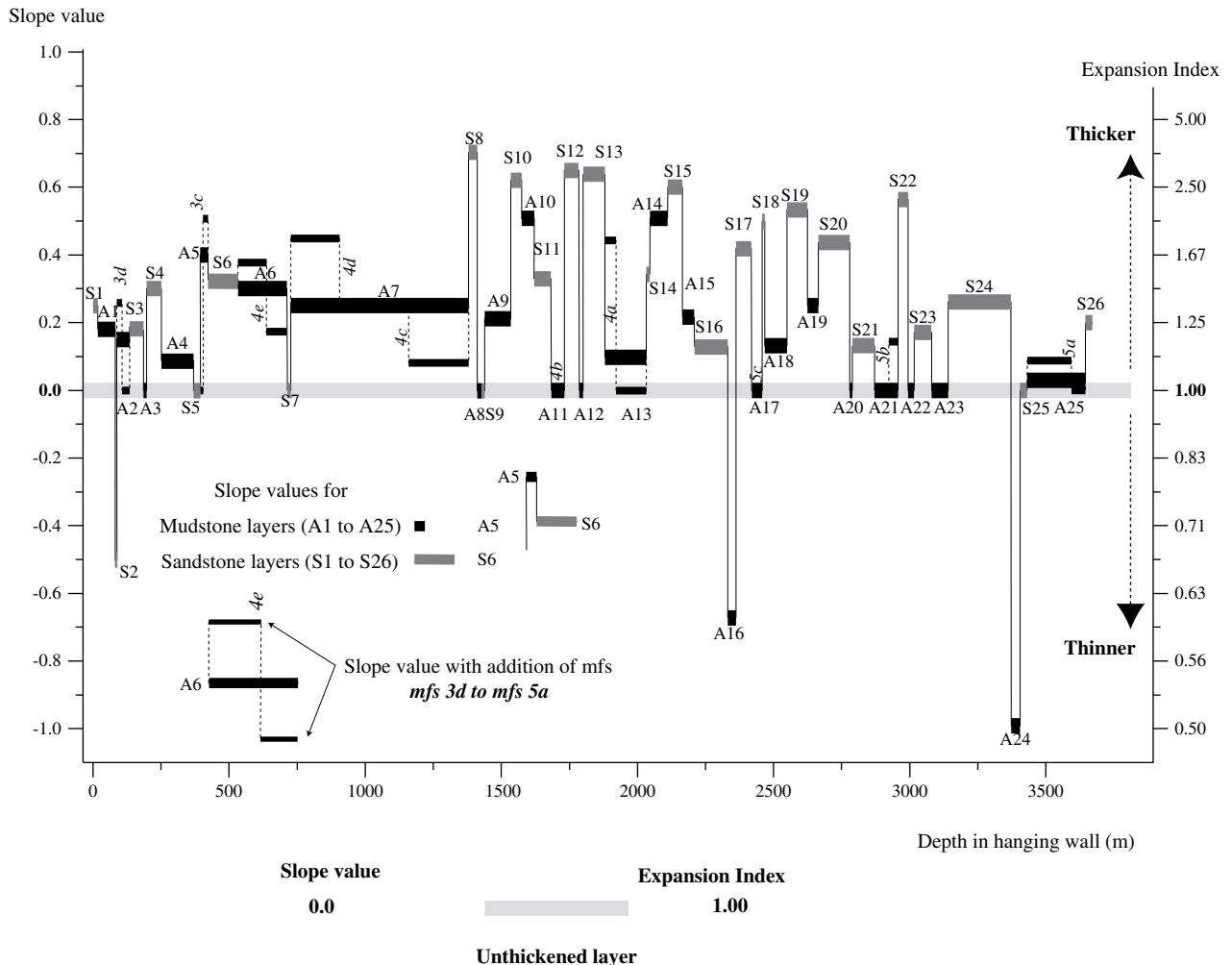


Fig. 8. Evolution of the slope of Th–z plot curve according to the depth of each marker in the hanging wall. We have reported the slope of the Th–z plot curve without (in bold line) and with the additional cutting with the mfs (dotted line). This composite curve will be used for the continuation.

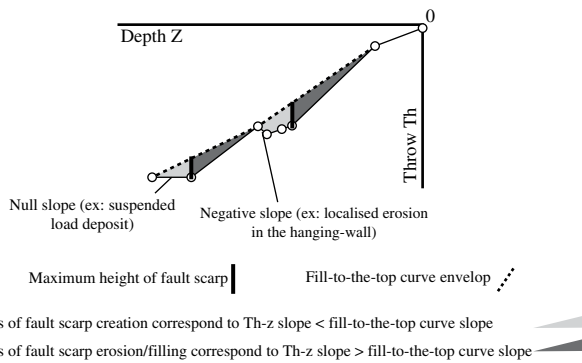


Fig. 9. Model of construction of “fill-to-the-top” curve from a Th–z plot curve (Castelltort et al., 2004a, b). a) Construction of the “fill-to-the-top” envelop curve, the “fill-to-the-top” model is only valid along this curve. The bolded line corresponds to the “fill-to-the-top” envelop curve, the dotted line corresponds to the initial Th–z plot. b) Extraction of the period of fault topographies or scarp creation in grey. The maximum vertical difference between the “fill-to-the-top” envelop curve and the initial Th–z plot gives the maximum height of the fault topographies.

differential of thickness variation between two adjacent layers is between shaly layer A8 and sandy layer S8 for a value of 350%.

8. Summary

The combined analysis of slope and lithological variations on the Th–z plot indicates that:

- 1) each lithological variation is associated with a change of slope;
- 2) the mudstone layers are generally thinned or unthickened in the hanging wall;
- 3) the sandstone layers are generally thickened in the hanging wall.

The “fill-to-the-top” model excludes the consideration of fault topographies and scarp creation. Interpreting the present case study in the framework of the fill-to-the-top model would lead to associate the systematic short-term slope variations observed here to systematic short-term changes of the fault movement rate of up to one order of magnitude (Fig. 8). The 17 zero-slope intervals would imply 17 periods of fault quiescence and the 3 negative slope intervals would indicate 3 periods of fault inversion or linkage. Such erratic behaviour of this normal fault is in contradiction with (1) the observed long-term continuous fault displacement (Fig. 6) and (2) the short-term ductile behaviour of the décollement layer (Morley and Guerin, 1996).

9. New model of Th–z plot interpretation

Instead of interpreting all slope changes as purely tectonically driven, an alternative solution is that every short-term slope variation rather indicates changes between periods of creation of topography on the fault and periods of fault topography erosion or filling (Castelltort et al., 2004a, b; Pochat et al., 2004).

Following this perspective, the fault topography at each instant can be different from zero and cannot be further neglected in such analysis. It follows that slope variation in Th–z plot variations no longer represents only displacement but a combination of fault displacement rate and remnant fault topography (Bischke, 1994; Castelltort et al., 2004a, b; Pochat et al., 2004). The general expression of α_i the slope of the Th–z plot on any interval where Δe_i is the variation of topography, d_i the incremental displacement and HW_t the thickness of the deposit in the hanging wall, is:

$$\alpha_i = \frac{d_i - \Delta e_i}{HW_t} \quad (3)$$

For a constant displacement d_i , the slope increases when topography diminishes (Fig. 9). As a consequence, on a Th–z plot, the points which follow the stronger slopes may be interpreted with confidence as representing low to zero topography. By contrast, between two of such points, the other points follow lower or even negative slopes and result from the creation of topography (Fig. 9).

Therefore, on any Th–z plots, one can draw straight segments between the points of assumed low topography, starting from the origin of the Th–z plot to the older horizon (Fig. 9). Important conclusions of this model are that (1) the slope of each of these segments represents the mean displacement rate relative to the sedimentation rate on the considered interval, and (2) the vertical deviations of the Th–z curve with respect to these segments represent creation of fault-induced topography (shaded areas in Fig. 9) (Castelltort et al., 2004a, b; Pochat et al., 2004). A “fill-to-the-top sedimentation” is implicitly assumed to work at the resolution of the chosen segments, and topographies occur at a higher frequency due to sedimentation changes. The only condition to respect when choosing intervals of steady growth is that there should be no point of any interval situated below the corresponding segment. Indeed, such a situation would imply a negative topography at the time of deposition of the considered horizon (i.e. horizon topographically higher in the hanging wall than on the footwall), which is unlikely. The Th–z plot thus contains the magnitude of the displacement on the fault at the segment resolution (interval), and the evolution of topography at each instant within the deviation of the curve from the segments (Fig. 9).

From the initial Th–z plot curve, by respecting the conditions previously defined, we built the “fill-to-the-top” curve envelope, depending on the configuration of the Th–z plot curve, it is sometimes possible to define two “fill-to-the-top” curves which are integrated as a degree of variability in the “fill-to-the-top” curve creation (Figs. 10 and 11). We calculate the slope variation in the “fill-to-the-top” envelope curve and report it on the slope variation diagram (Fig. 11). The existence of a vertical space between both curves defines periods of fault scarp creation and periods of filling and/or erosion of fault scarps. Thus each slope inferior to the slope of the “fill-to-the-top” curve envelop corresponds to a fault topography creation period, each slope superior to the slope of the “fill-to-the-top” curve envelop correspond to a fault topography destruction period (predominantly filling or erosion) (Fig. 11). We thus determine 18 periods of fault scarp creation which are generally associated with mud deposits for 22 (75%) layers out of 29 (Figs. 11 and 12).

Between the “fill-to-the-top” curve and the Th–z plot curve, the maximum vertical space allows us to estimate the maximum height of the fault scarps (Castelltort et al., 2004a, b; Pochat et al., 2004). For the periods with two possible “fill-to-the-top” curves we give two possible values of fault scarp heights (Fig. 10–12). Thus the heights of the fault scarps are between 5 and 40 m (Fig. 12a), the cumulative fault scarp height is ranging from 340 to 355 m which represents 40–45% of the total throw along the fault. The values of fault scarp relief are consistent with observations of fault scarps on the current sea floor in similar sedimentary and tectonic settings as in the Mississippi river delta (Coleman and Prior, 1978, 1981), in the Baram river delta (Hiscott, 2001) and in the Niger river delta (Damuth, 1994; Cohen and McClay, 1996a, b; Armentrout et al., 2000; Adeogba et al., 2005).

The longest period of maximum fault scarp creation is located during the early history of the fault movement (Fig. 12b). Here the rate of fault scarp creation are around 70% (0.7) of the rate of the

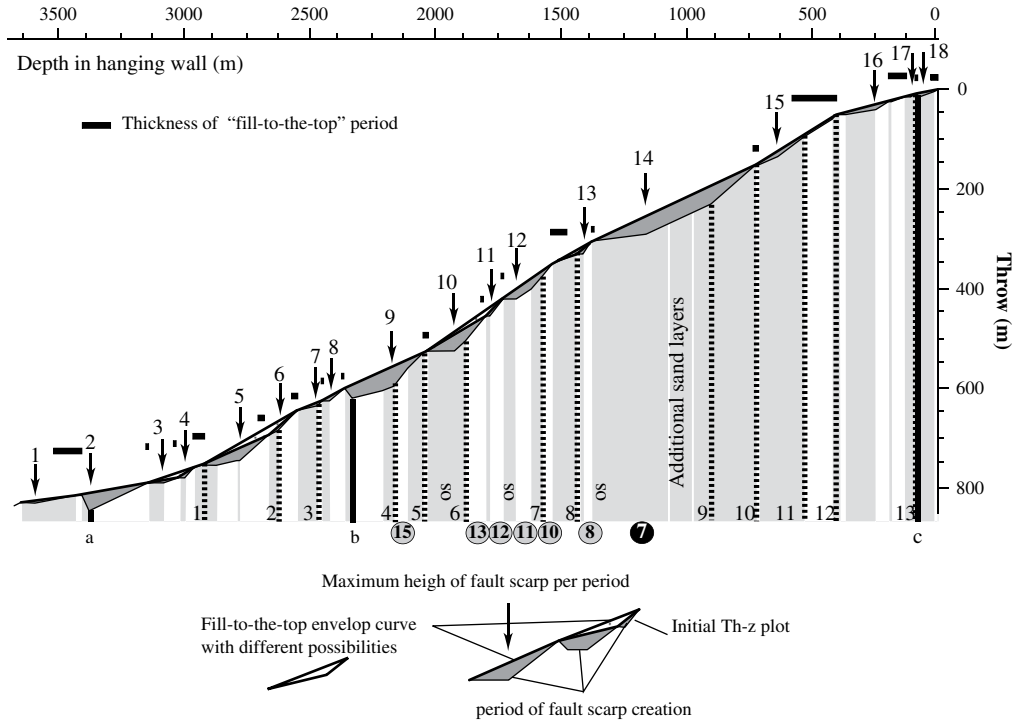


Fig. 10. Construction of the “fill-to-the-top” curve from the initial Th-z plot curve and determination of the fault scarp creation periods. The vertical space between both curve indicate periods of fault scarp creation and persistence. There are 18 periods of fault scarp creation which are indicate by black vertical arrows. For a better reading the height of every fault scarp will be given in Fig. 12. Bold line with letters a–b–c correspond to possible period of flow canalisation and erosion in the hanging wall of which two (a and b, base of S24 and S16) are described as regional erosive events. Dotted lines with numbers 1–13 correspond to possible period of localized erosion on the footwall in mudstone layers. White circles with black numbers correspond to additional sandstone layers (thickness > 1 m) inside mudstone deposits in the hanging wall, black circles with white numbers correspond to additional shale layers (thickness > 1 m) inside sand deposits in the hanging wall. These additional levels in the hanging wall are symptomatic of preferential filling of fault topographic lows and thus here of the existence of fault scarp during sedimentation. The black boxes along the curve indicate periods (between 12 and 19 periods) of fault scarp non-appearance during fault movement i.e. a true “fill-to-the-top” behaviour.

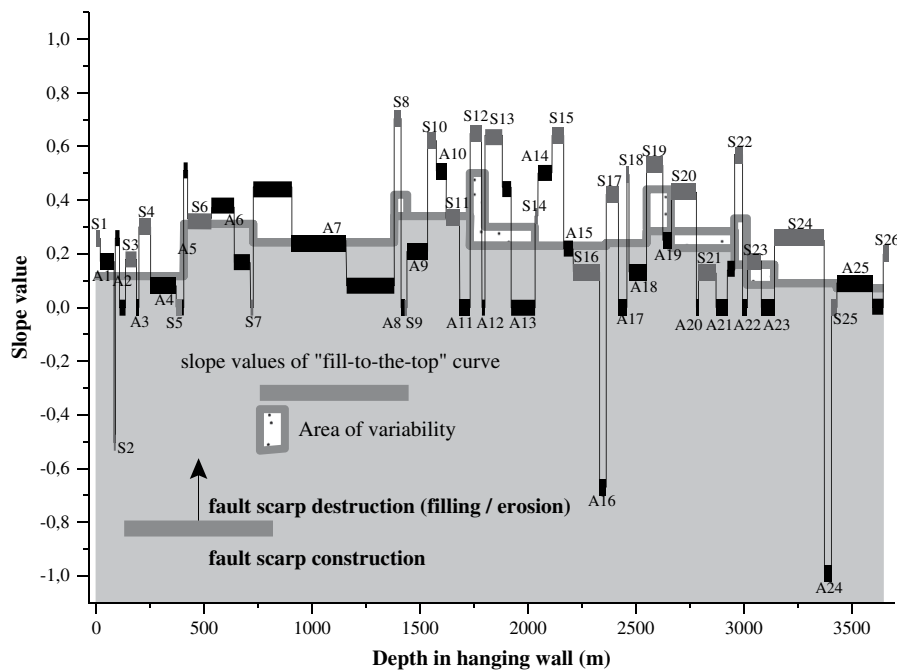


Fig. 11. Comparison of Th-z slope variation and “fill-to-the-top” curve slope variation as indicator of period fault scarp construction and destruction. The evolution of the slope of Th-z plot curve according to the depth of each marker in the hanging wall with addition of the slope values of the “fill-to-the-top” curve. Each part of the Th-z curve located below the “fill-to-the-top” curve has to be associated with a period of fault scarp construction, each part of the Th-z curve located above the “fill-to-the-top” curve has to be associated with a period of fault destruction (filling or erosion). If both curves are merged, no fault scarp are created or destroyed.

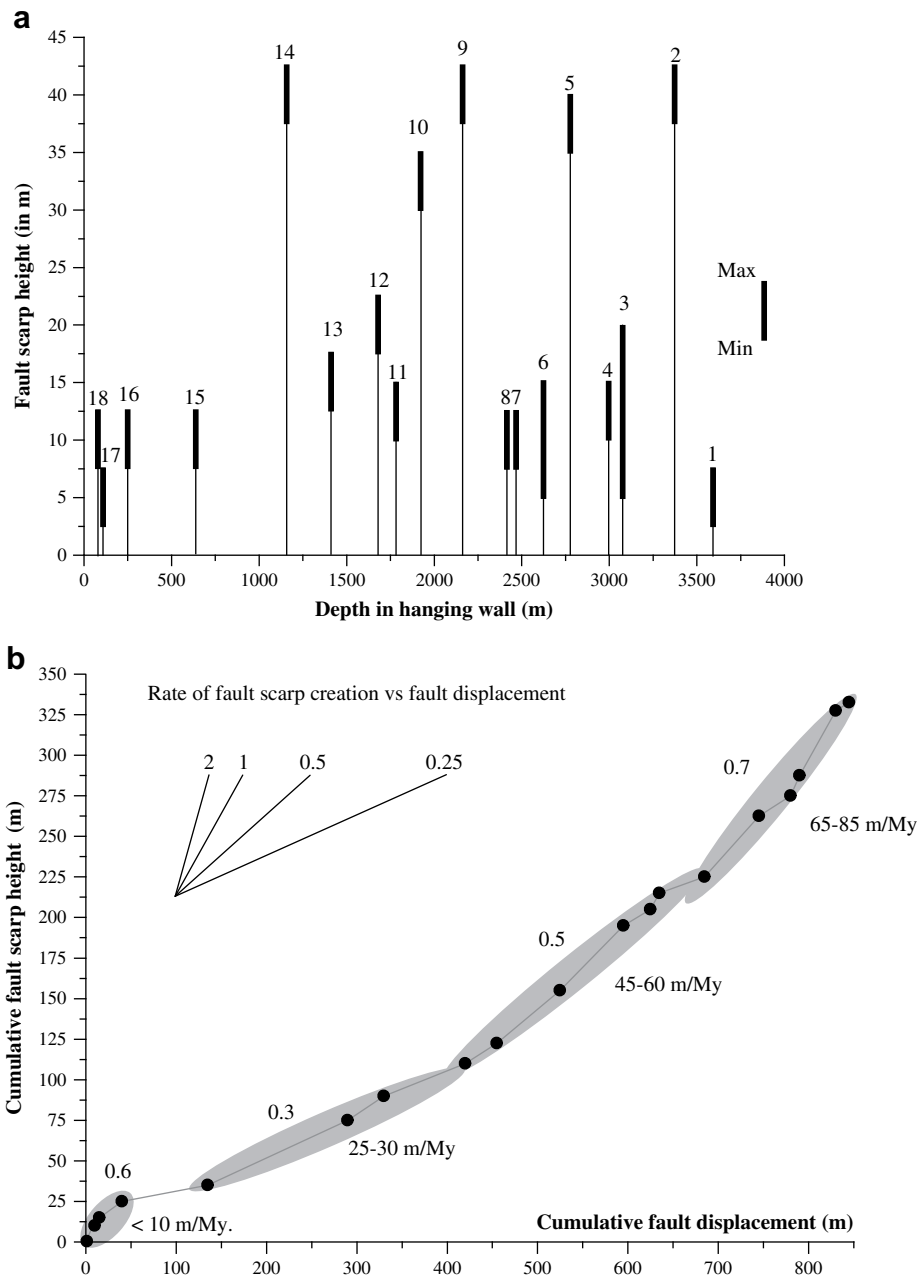


Fig. 12. Quantification of fault scarp height a) Evolution of the maximum height of fault scarp per period plotted against their position in the hanging wall. b) Evolution of the cumulative fault scarp height plotted against the cumulative fault displacement. A slope equal to 1 (100%) indicates a rate of fault scarp creation equal to the rate of the fault scarp displacement. From the left to the right, we observe 4 main sectors with slope evolve from 0.7 (70%), 0.5 (50%), 0.3 (30%) and 0.6 (60%). By multiplying these rates by fault displacement rate i.e. from 90–120 m/My to 10–15 m/My, we obtain a gradual decrease of the fault scarp creation rate from 65–85 m/My to 45–60 m/My to 25–30 m/My to a value inferior to 10 m/My.

fault displacement (Fig. 12b) which means that 70% of the fault movement are expressed at the Earth surface or on sea floor in term of fault scarp. The rate of fault scarp creation gradually decreases from 50% to 30% but with a new increase to 60% at the end of the curve (Fig. 12b). We have transform these rates into a rate of fault scarp creation by using the fault displacement rate previously calculated (see Fig. 6). Thus we obtain a gradual decrease of the fault scarp creation rate from 65–85 m/My to 45–60 m/My to 25–30 m/My to a value inferior to 10 m/My (Fig. 12b).

We have also observed that the vertical displacement of the fault are not entirely expressed in fault scarp creation at the Earth surface or on the sea floor. This absence of fault scarp is observable when the

Th–z plot curve and “fill-to-the-top” curve are nearly or totally merged (Fig. 10). These segments indicate 19 periods of non-appearance of fault scarp on the sea floor (Fig. 10) when the fault was constantly active which corresponds to a “fill-to-the-top” model.

10. Model of fault scarp creation and its sedimentary consequences

We propose that fault topography creation is preferentially associated with clay deposition by suspended-load processes, which allow the preservation of a fault-induced topography on the sea floor. Conversely, sand transport by bedload processes will

preferentially fill up and smooth fault-related topographies on the sea floor. During periods of suspended-load deposition (preferentially during transgressive and early highstand sea levels), the fault scarp and fault trough can stay preserved rather than filled by sediments. On the other hand, during periods of bedload deposition (preferentially during late highstand and falling sea level), the fault scarp and fault trough can become filled more quickly than rejuvenated. Thus, transgressive periods with dominant suspended load deposition (shale) and/or low rate of sedimentation in offshore environments will favour the expression of fault-induced topographies on the sea floor (Hiscott, 2001), whereas regressive periods with dominant bedload (sand) and/or high rate of sedimentation will favour filling up or erosion and smoothing of sea floor topographies created by faulting. The fact that fault-induced topography is filled up is confirmed by abundance of extra layers in the hanging wall (Fig. 10) see also Hodgetts et al. (2001). Given that the initial precision of data (1 m), it is highly probable that extra layers of thickness inferior than 1 m are distributed anywhere in the lithological column.

The presence of negative slopes is usually associated with strong erosion surfaces in the hanging wall as for mudstone layers 24 and

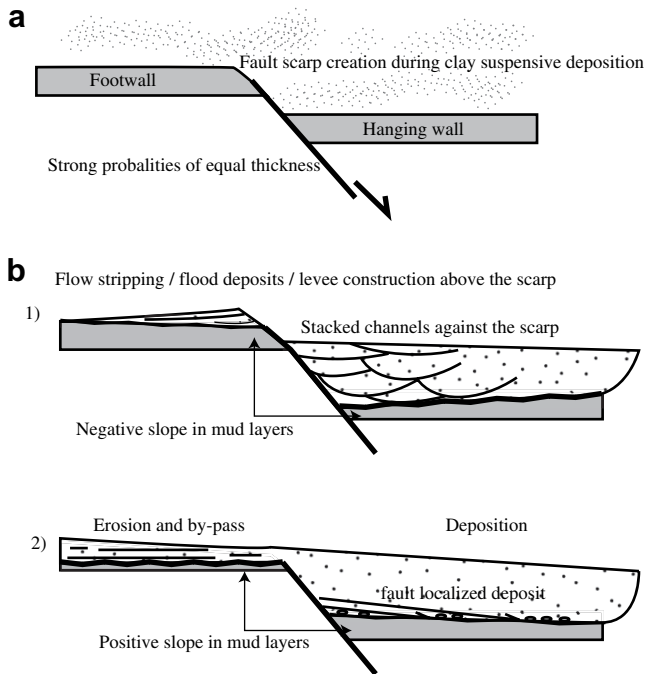


Fig. 13. Model of fault scarp creation and filling during a continuous fault displacement. a) Fault scarp creation is facilitated during the periods dominated by clay/mud suspensive-load deposits (highstand periods). b) Erosion phenomena associated with bedload processes, can modify the initial distribution of the mud thicknesses above the fault into two possible ways. 1) If flow thickness are smaller than fault scarp height: the flow can be deviated or captured along to fault scarp or concentrated only in the hanging wall with small impact on the footwall. Some sedimentary features can be associated with this phenomenon such as stacked channels along the fault with their large axis parallel to the fault. In this case, we should observe large discontinuity into facies distribution and lithological composition of deposits above the scarp with the preservation of infrequent deposit on the footwall (large flood in fluvial settings, flow stripping in subaqueous sediment gravity flows). 2) If flow thickness at the same or higher scale than fault scarp height it may induces flow disturbances over the footwall with enhanced erosion phenomena on this compartment (e.g. Edwards, 1995; Morris et al., 1998; Pochat and Van Den Driessche, 2007). If the flow comes from the hanging wall or from the footwall it may induces different response of the sedimentary processes. We may observe, for example, a brutal transition from fault-localized ripples or dunes in the hanging wall to planar lamination, strong basal erosion on the footwall, high concentration of mud intraclasts and coarse to very coarse granulometry due to fault scarp degradation.

16 (a and b in Fig. 11). They indicate that the thickness of the hanging-wall layers is inferior to its counterpart on the footwall. In a case of a continuous fault displacement it can also be explain by sedimentary processes. Indeed the presence of a fault topographies on sea-bed or at earth surface can induce flow channelization, deviation or transformation along and/or again the scarp (see reference in Introduction part) (Fig. 13). For example, flow channelization or flow capture along the fault scarp can be accompanied by localized erosion at the base of scarp in the hanging wall (Fig. 13). Flow channelization or transformation in the hanging wall due to the presence of fault scarps may enhance flow transformation against the obstacle and induce particular sediment deposits on the footwall (Fig. 13). For example, in submarine settings, fault scarp may induce flow stripping processes flow channelization and erosion in lows and deposition on highs (e.g. Piper and Normark, 1983; Anderson et al., 2000; Armentrout et al., 2000). In this case, deposits in the hanging wall should be accompanied by fault-parallel paleocurrent direction, amalgamated channel belt along the scarp (submarine, deltaic, fluvial...) (Fig. 13).

Positive slopes associated with mudstone layers correspond to intervals where shales deposits are thickened in the hanging wall and could therefore be due to particular periods of erosion localized over the footwall which is the most commonly described case in the impact of fault scarps on sedimentation (e.g. Edwards, 1995; Morris et al., 1998; Pochat and Van Den Driessche, 2007). Thus, we proposed that all positive-slope associated with mudstone layers (13 layers) (Fig. 11) indicate localized erosion surface at the top or inside of each mudstone layers on the footwall with less even no erosion in the hanging wall (Fig. 13). In this case, deposits in the hanging wall can be accompanied with for example downstream-oriented fault-localized oblique lamination associated with high concentration of mud intraclasts (Fig. 13) (Pochat and Van Den Driessche, 2007).

In any case, strong thickness variation inside mudstone layers due to fault scarp impact on flow dynamics and subsequent erosion will be necessarily associated with large facies variation across the same fault of the overlying sandstone deposit i.e. large variation of reservoir properties over small distance (Fig. 13).

11. Conclusion

Analysis of kinematics of a synsedimentary normal fault in the Niger delta based on throw versus time method has provided a long-term evolution characterized by continuous slip of 0.1 mm/y during 10 millions of years. Such stable fault growth, and related displacement rates, can appear punctuated when viewed at the scale of sedimentary cycles.

At such times scale, the Th–z plot diagram reveal that sand deposits are always much thicker within the hanging wall than in the footwall. By contrast, mudstone deposits are either only weakly thickened in the hanging wall or have a similar thickness on each side of the fault. The sand intervals are proportionally more thickened than the mudstone intervals. Classical “fill-to-the-top” interpretation of thickness variation of growth strata would lead to the erroneous conclusion of alternation of fault activity and fault quiescence and even of fault inversion, which is highly unlikely given the gravity sliding context. Such alternation is moreover in contradiction with the long-term evolution as documented by the throw versus time method. The polycyclic fault behaviour diagnosed for some faults at the scale of sedimentary cycles is most probably an artefact of the fill-to-the-top method and may instead be entirely related to varying sedimentation rates. The high quality data presented here also provide strong grounds for supporting the notion that fault displacement rates can be very well behaved (e.g. Nicol et al., 1997, 2005; Meyer et al., 2002; Walsh et al., 2002; Mouslopoulou et al., 2009).

A more suitable approach is to carefully take into account sedimentation processes. Mudstone intervals correspond to dominant suspended-load processes that result in the preservation of fault scarps whereas sand intervals are created by dominant bedload processes that result in the filling and smoothing of the fault-related topographies. Negative slope can be related to flow channelization and erosion in the hanging wall. The present example shows that the variations of the growth strata thickness that reflect the alternation of fault-induced scarp creation and fault scarp sealing in deltaic gravity tectonics settings are controlled by sedimentation dynamics during continuous fault slip rather than by pulsating fault activity. In the future, such kind of analysis must include a 3D quantification along and perpendicular to the fault plane orientation of (1) the sedimentary processes and facies evolution and (2) the throw variation.

Eventually, along a synsedimentary fault, displacement analysis at scales larger than alternating sedimentological processes (<1 m) and high-frequencies stratigraphic cycle (up to ~ several m) will be more suited to reveal the continuous nature of fault activity. Moreover, analysis at the scales of alternating sedimentological processes and high-frequencies stratigraphic cycle along synsedimentary fault can reveal the nature of the sedimentary processes in relation to sequence stratigraphic states.

Acknowledgments

Stephane Pochat gratefully acknowledges Total for the data provided during its PhD thesis. Jean Van Den Driessche, Gael Choblet have enjoyed financial support from the French National Center for Scientific Research (CNRS). Sebastien Castellort has enjoyed financial support from ETH-Zurich. Many thanks to J.J. Walsh for its very helpful and enthusiastic review and to Craig Jonathan for its professionalism despite the difficulties. The authors warmly thank Nadine, Norbert and Sandrine Castellort for their permanent hospitality under the Viala's cantou. In honor to Pierre Desproges, the visionary, who has predicted 30 years ago the current problems of the French research "because the peoples of French Brittany don't want to collaborate with science". Please do not forget that sciences, as art, is not just a consumable.

Appendix A. Method of decompaction

In order to compute the decompacted thicknesses of the various sediment layers, we have adapted a simple procedure from [Sclater and Christie \(1980\)](#). Assuming an exponential relationship between porosity ϕ and depth z :

$$\phi = \phi_0 \exp(-cz) \quad (1)$$

the volume of water Z_w in a given sediment layer between Z_{top} and Z_{bot} (for a cross-section with a unit area) is

$$Z_w(z_{top}, z_{bot}) = \phi_0/c \left(\exp(-cz_{top}) - \exp(-cz_{bot}) \right) \quad (2)$$

The volume conservation of a porous sediment layer with thickness ($Z_{top}-Z_{bot}$) exhumed from depth Z_{top} to depth Z'_{top} then implies

$$Z'_{top} - Z'_{bot} + Z_w(z_{top}, z_{bot}) = Z_{top} - Z_{bot} + Z_w(z_{top}, z_{bot}) \quad (3)$$

so that the new thickness ($Z'_{top}-Z'_{bot}$) of a layer culminating at depth Z'_{top} is easily obtained. Repeating step by step a procedure where a new depth Z'_{top} results from the decompaction of a layer that is shallower in the sedimentary column thus leads to the 'decompacted thickness' of the whole column.

In the present study, we describe the compaction process with an additional parameter corresponding to the 'stride' of sediment loading: instead of using eq. (3) with (Z_{top}, Z_{bot}) corresponding to the vertical limits of the layer, we subdivide this layer with the incremental thickness Z_{inc} and perform the integration with this value. A simple algorithm based on the classical Newton–Raphson method is used to find the zero of eq. (3) for each sublayer.

References

- Adeogba, A.A., McHargue, T.R., Graham, S.A., 2005. Transient fan architecture and depositional controls from near-surface 3-D seismic data, Niger Delta continental slope. *American Association of Petroleum Geologists Bulletin* 89 (5), 627–643.
- Anderson, J.E., Cartwright, J., Drysdall, S.J., Vivian, N., 2000. Controls on turbidite sand deposition during gravity-driven extension of a passive margin: examples from Miocene sediments in Block 4, Angola. *Marine and Petroleum Geology* 17 (10), 1165–1203.
- Armentrout, J.M., et al., 2000. Neogene turbidite systems of the Gulf of Guinea continental margin slope, offshore Nigeria. In: Bouma, A.H., Stone, C.G. (Eds.), *Fine-grained Turbidite Systems*. Society of Economic Paleontologists and Mineralogists, Special Publication 68, Memoir 72. American Association of Petroleum Geologists, pp. 93–108.
- Back, S., Hocker, C., Brundiers, M.B., Kukla, P.A., 2006. Three-dimensional-seismic coherency signature of Niger Delta growth faults: integrating sedimentology and tectonics. *Basin Research* 18 (3), 323–337.
- Baudon, C., Cartwright, J., 2008. The kinematics of reactivation of normal faults using high resolution throw mapping. *Journal of Structural Geology* 30 (8), 1072–1084.
- Beach, A., 1984. Structural evolution of the Witch Ground Graben. *Journal of the Geological Society of London* 141 (JUL), 621–640.
- Berggren, W.A., Kent, D.V., Swisher, C.C., Aubry, M.-P., 1995. A revised Cenozoic geochronology and chronostratigraphy. In: Berggren, W.A., Kent, D.V., Aubry, M.-P., Hardenbol, J. (Eds.), *Geochronology, Time Scales and Global Stratigraphic Correlation*. Society of Economic Paleontologists and Mineralogists, Tulsa, pp. 95–126.
- Bhattacharya, J.P., Davies, R.K., 2001. Growth faults at the prodelta to delta-front transition, Cretaceous Ferron sandstone, Utah. *Marine and Petroleum Geology* 18, 525–534.
- Bischke, R.E., 1994. Interpreting sedimentary growth structures from well log and seismic data (with examples). *American Association of Petroleum Geologists Bulletin* 78 (6), 873–892.
- Brown, L.F., Loucks, R.G., Trevino, R.H., Hammes, U., 2004. Understanding growth-faulted, intraslope subbasins by applying sequence-stratigraphic principles: examples from the south Texas Oligocene Frio Formation. *American Association of Petroleum Geologists Bulletin* 88 (11), 1501–1522.
- Bruce, C.H., 1973. Pressured shale and related sediment deformation: mechanism for development of regional contemporaneous faults. *American Association of Petroleum Geologists Bulletin* 57 (5), 878–886.
- Burke, K.C.B., 1972. Longshore drift, submarine canyons, and submarine fans. *American Association of Petroleum Geologists Bulletin* 56, 1975–1983.
- Cartwright, J.A., Bouroulec, R., James, D., Johnson, C.S., 1998. Polycyclic motion history of some Gulf Coast growth fault from high resolution displacement analysis. *Geology* 26, 819–822.
- Castellort, S., Pochat, S., Van Den Driessche, J., 2004a. How reliable are growth strata in interpreting short-term (10 s to 100 s ka) growth structures kinematics? *Comptes Rendus Geosciences* 336 (2), 151–158.
- Castellort, S., Pochat, S., Van Den Driessche, J., 2004b. Using T–Z plots as a graphical method to infer lithological variations from growth strata. *Journal of Structural Geology* 26 (8), 1425–1432.
- Childs, C., et al., 1993. Kinematic analysis of faults in a physical model of growth faulting above a viscous salt analogue. *Tectonophysics* 228 (3–4), 313–329.
- Childs, C., Nicol, A., Walsh, J.J., Watterson, J., 2003. The growth and propagation of synsedimentary faults. *Journal of Structural Geology* 25 (4), 633–648.
- Chukwueke, C., Thomas, G., Delfaud, J., 1992. Processus sédimentaires, eustatisme, subsidence et flux thermique dans la partie distale du Delta du Niger. *Bulletin des Centres de Recherches Exploration-Production Elf-Aquitaine* 16 (1), 137–186.
- Cohen, H.A., McClay, K., 1996a. Sedimentation and shale tectonics of the north-western Niger Delta front. *Marine and Petroleum Geology* 13 (3), 313–328.
- Cohen, H.A., McClay, K.R., 1996b. Niger Delta shale tectonics. *Marine and Petroleum Geology* 11, 313–328.
- Coleman, J.M., Prior, D.B., 1978. Contemporary gravity tectonics – everyday catastrophe. *American Association of Petroleum Geologists Bulletin* 62 (3), 505.
- Coleman, J.M., Prior, D.B., 1981. Deltaic influence on shelf-edge instability processes. *American Association of Petroleum Geologists Bulletin* 65 (5), 912.
- Crans, W., Mandl, G., Haremboure, J., 1980. On the theory of growth faulting: a geomorphological delta model based on gravity sliding. *Journal of Petroleum Geology* 2–3, 265–307.
- Cross, T.A., Lessinger, M.A., 1998. Sediment volume partitioning: rationale for stratigraphic model evaluation and high-resolution stratigraphic correlation. In: Gradstein, F.M., Sandvik, K.O., Milton, N.J. (Eds.), *Sequence Stratigraphy* –

- Concepts and Applications. Norwegian Petroleum Society (NPF), Special Publications. Elsevier, pp. 171–195.
- Damuth, J.E., 1994. Neogene gravity tectonics and depositional processes on the deep Niger Delta continental margin. *Marine and Petroleum Geology* 11, 320–346.
- Dawers, N.H., Underhill, J.R., 2000. The role of fault interaction and linkage in controlling synrift stratigraphy sequences: late Jurassic, Stratford East Area, Northern North Sea. *American Association of Petroleum Geologists Bulletin* 84 (1), 45–64.
- Dogliani, C., D'Agostino, N., Mariotti, G., 1998. Normal faulting vs regional subsidence and sedimentation rate. *Marine and Petroleum Geology* 15, 737–750.
- Doust, H., 1990. Petroleum geology of the Niger Delta. In: Brooks, J. (Ed.), *Classic Petroleum Provinces*. Geological Society, Special Publication, p. 365.
- Doust, H., Omatsola, E., 1990. Niger Delta. In: Edwards, J.D., Santogrossi, P.A. (Eds.), *Divergent/Passive Margins Basins*. American Association of Petroleum Geologists Memoir, pp. 201–238.
- Dula, W.F., 1991. Geometric models of listric normal faults and rollover folds. *American Association of Petroleum Geologists Bulletin* 75 (10), 1609–1625.
- Edwards, M.B., 1976. Growth faults in Upper Triassic deltaic sediments. *American Association of Petroleum Geologists Bulletin* 60 (3), 341–355.
- Edwards, M.B., 1995. Differential Subsidence and Preservation Potential of a Shallow Water Tertiary Sequences, vol. 22. International Association of Sedimentologists, Special Publication, Northern Gulf Coast Basin, USA, pp. 265–281.
- Gagliano, S.M., Kemp, E.B., Wicker, K.M., Wiltenmuth, K.S., 2003. New tectonic framework of southeastern Louisiana and applications to coastal restoration. *Transactions of the Gulf Coast Association of Geological Societies* 53, 262–276.
- Gaullier, V., Vendeville, B.C., 2005. Salt tectonics driven by sediment progradation: part II – radial spreading of sedimentary lobes prograding above salt. *American Association of Petroleum Geologists Bulletin* 89 (8), 1081–1089.
- Ge, H.X., Jackson, M.P.A., Vendeville, B.C., 1997. Kinematics and dynamics of salt tectonics driven by progradation. *American Association of Petroleum Geologists Bulletin* 81 (3), 398–423.
- Gibbs, A.D., 1983. Balanced cross-section construction from seismic sections in areas of extensional tectonics. *Journal of Structural Geology* 5 (2), 153–160.
- Hardenbol, J., et al., 1998. Mesozoic and Cenozoic sequence chronostratigraphic framework of European basins, chart 1. In: DeGraciansky, P.C., Hardenbol, J., Jacquin, T., Vail, P.R. (Eds.), *Mesozoic and Cenozoic Sequence Stratigraphy of European Basins*. Society of Economic Paleontologists and Mineralogists, Special Publication.
- Hardin, F.R., Hardin, G.C., 1961. Contemporaneous normal fault of Gulf Coast and their relation to flexures. *American Association of Petroleum Geologists Bulletin* 45 (2), 238–248.
- Hardy, S., McClay, K., 1999. Kinematic modelling of extensional fault-propagation folding. *Journal of Structural Geology* 21, 695–702.
- Heinio, P., Davies, R.J., 2007. Knickpoint migration in submarine channels in response to fold growth, western Niger Delta. *Marine and Petroleum Geology* 24 (6–9), 434–449.
- Hiscott, R.N., 2001. Depositional sequences controlled by high rates of sediment supply, sea-level variations, and growth faulting: the Quaternary Baram Delta of northwestern Borneo. *Marine Geology* 175, 67–102.
- Hodgetts, D., et al., 2001. Sequence stratigraphic responses to shoreline-perpendicular growth faulting in shallow marine reservoirs of the Champion field, offshore Brunei Darussalam, South China Sea. *American Association of Petroleum Geologists Bulletin* 85 (3), 433–457.
- Hodgson, D.M., Haughton, P.D.W., 2004. Impact of Syndepositional Faulting on Gravity Current Behaviour and Deep-water Stratigraphy, vol. 222(1). Geological Society, London, Special Publications, Tabernas-Sorbas Basin, SE, Spain, pp. 135–158.
- Hooper, J.R., Fitzsimmons, R.J., Grant, N., Vendeville, B.C., 2002. The role of deformation in controlling depositional patterns in the south-central Niger Delta, West Africa. *Journal of Structural Geology* 24, 847–859.
- Jackson, J.A., White, N.J., 1989. Normal faulting in the upper continental-crust – observations from regions of active extension. *Journal of Structural Geology* 11 (1–2), 15–36.
- Koyi, H., 1991. Gravity overturns, extension, and basement fault activation. *Journal of Petroleum Geology* 14 (2), 117–142.
- Koyi, H., Jenyon, M.K., Petersen, K., 1993. The effect of basement faulting on Diapirism. *Journal of Petroleum Geology* 16 (3), 285–311.
- Leeder, M.R., Jackson, J., 1993. The interaction between normal faulting and drainage in active extensional basins, with examples from the western United States and Central Greece. *Basin Research* 5, 79–102.
- Loncke, L., Gaullier, V., Mascle, J., Vendeville, B., Camera, L., 2006. The Nile deep-sea fan: an example of interacting sedimentation, salt tectonics, and inherited subsalt paleotopographic features. *Marine and Petroleum Geology* 23 (3), 297–315.
- Lowrie, A., 1986. Model for fine-scaled movements associated with climate and sea-level changes along Louisiana shelfbreak growth faults. *Transactions of the Gulf Coast Association of Geological Societies* 36, 497–509.
- Magbagbeola, O.A., Willis, B.J., 2007. Sequence stratigraphy and syndepositional deformation of the Agbada formation, Robertkiri field, Niger Delta, Nigeria. *American Association of Petroleum Geologists Bulletin* 91 (7), 945–958.
- Mansfield, C.S., Cartwright, J.A., 1996. High resolution displacement mapping from 3-D seismic data. *Journal of Structural Geology* 18, 249–263.
- Mauduit, T., Brun, J.P., 1998. Growth fault/rollover systems: birth, growth and decay. *Journal of Geophysical Research* 103, 18119–18136.
- Mauduit, T., Guerin, G., Brun, J.P., Lecanu, H., 1997. Raft tectonics: the effects of basal slope angle and sedimentation rate on progressive extension. *Journal of Structural Geology* 19 (9), 1219–1230.
- Merki, P., 1972. Structural geology of the Cenozoic Niger Delta. In: Dessauvage, T.F.J., Whiteman, A.J. (Eds.), *African Geology*. Ibadan University Press, pp. 635–646.
- Meyer, V., Nicol, A., Childs, C., Walsh, J.J., Watterson, J., 2002. Progressive localisation of strain during the evolution of a normal fault population. *Journal of Structural Geology* 24 (8), 1215–1231.
- Mitchell, N.C., 1996. Creep in pelagic sediments and potential for morphologic dating of marine fault scarps. *Geophysical Research Letters* 23, 483–486.
- Mitchum, R.M., Van Wagoner, J.C., 1991. High-frequency sequences and their stacking patterns – sequence stratigraphic evidence of high-frequency eustatic cycles. *Sedimentary Geology* 70 (2–4), 131–160.
- Morley, C.K., Guerin, G., 1996. Comparison of gravity-driven deformation styles and behavior associated with mobile shales and salt. *Tectonics* 15 (6), 1154–1170.
- Morley, C.K., Vanhauwaert, P., De Batist, M., 2000. Evidence for high-frequency cyclic activity from high-resolution seismic reflection survey, Rukwa Rift, Tanzania. *Journal of the Geological Society of London* 157, 983–994.
- Morris, S.A., Alexander, J., Kenyon, N.H., Limonov, A.F., 1998. Turbidites around an active fault scarp on the Lower Valencia Fan, northwest Mediterranean. *Geo-Marine Letters* 18, 165–171.
- Mouslopoulou, V., Walsh, J.J., Nicol, A., 2009. Fault displacement rates on a range of timescales. *Earth and Planetary Science Letters* 278 (3–4), 186–197.
- Newell, A.J., 2000. Fault activity and sedimentation in a marine rift basin (Upper Jurassic, Wessex basin, UK). *Journal of the Geological Society of London* 157 (1–2), 83–92.
- Nicol, A., Walsh, J.J., Manzocchi, T., Morewood, N., 2005. Displacement rates and average earthquake recurrence intervals on normal faults. *Journal of Structural Geology* 27 (3), 541–551.
- Nicol, A., Walsh, J.J., Watterson, J., Underhill, J.R., 1997. Displacement rates of normal faults. *Nature* 390, 157–159.
- Oakes, R.L., 1959. The Grandisson Complex, Lafourche and Jefferson Parishes, Louisiana. *Transactions of the Gulf Coast Association of Geological Societies* 4, 183–200.
- Ocamb, R.D., 1961. Growth fault of south Louisiana. *Transactions of the Gulf Coast Association of Geological Societies* 11, 139–175.
- Owoyemi, A.O., Willis, B.J., 2006. Depositional patterns across syndepositional normal faults, Niger Delta, Nigeria. *Journal of Sedimentary Research* 76 (1–2), 346–363.
- Petit, J.P., Beauchamp, J., 1986. Synsedimentary faulting and palaeocurrent patterns in the Triassic sandstones of the High Atlas (Morocco). *Sedimentology* 33, 817–829.
- Piper, D.J.W., Normark, W.R., 1983. Turbidite depositional patterns and flow characteristics, Navy Submarine Fan, California Borderland. *Sedimentology* 30, 681–694.
- Pochat, S., 2003. Synsedimentary fault scarps: Perturbation of sediment gravity flow and fault kinematics determination. Ph.D. Thesis, Rennes 1, 283 pp.
- Pochat, S., Castellort, S., Van Den Driessche, J., Besnard, K., Gumiaux, C., 2004. A simple method of determining sand/shale ratios from seismic analysis of growth faults: an example from upper Oligocene to lower Miocene Niger Delta deposits. *American Association of Petroleum Geologists Bulletin* 88, 1357–1367.
- Pochat, S., Van Den Driessche, J., 2007. Impact of syndepositional metre-scale normal fault scarps on sediment gravity flow dynamics: an example from the Gres d'Annot Formation, SE France. *Sedimentary Geology* 202 (4), 796–820.
- Price, N.J., 1977. Aspects of gravity tectonics and the development of listric faults. *Journal of the Geological Society of London* 133, 311–327.
- Schulbaum, L., Durand, J., Rousset, D., 1996. Traduction des surfaces stratigraphiques et des géométries deltaïques lors du passage de l'échelle puit à l'échelle sismique. *Bulletin de la Société Géologique de France* 167 (6), 667–683.
- Sclater, J.G., Christie, P.A.F., 1980. Continental stretching – an explanation of the post-Mid-Cretaceous subsidence of the Central North-Sea Basin. *Journal of Geophysical Research* 85 (B7), 3711–3739.
- Short, K.C., Stauble, A.J., 1967. Outline of geology of Niger Delta. *American Association of Petroleum Geologists Bulletin* 51, 761–779.
- Soreghan, M.J., Scholz, C.A., Wells, J.T., 1999. Coarse-grained, deep-water sedimentation along a border fault margin of Lake Malawi, Africa: seismic stratigraphic analysis. *Journal of Sedimentary Research* 69, 832–846.
- Taylor, S.K., Nicol, A., Walsh, J.J., 2008. Displacement loss on growth faults due to sediment compaction. *Journal of Structural Geology* 30 (3), 394–405.
- Tearpock, D., Bischke, R.E., 1991. *Applied Subsurface Geological Mapping*. Prentice-Hall, New-York, 648 pp.
- Thornburg, T.M., Kulm, L.D., Hussong, D.M., 1990. Submarine-fan development in the southern Chile Trench: a dynamic interplay of tectonics and sedimentation. *Geological Society of America Bulletin* 102, 1658–1680.
- Thorsen, C.E., 1963. Age of growth faulting in Southeast Louisiana. *Transactions of the Gulf Coast Association of Geological Societies* 13, 103–110.
- Van Wagoner, J.C., et al., 1988. An overview of the fundamentals of sequence stratigraphy and key definitions. In: Wilgus, C.K., Hastings, B.S., Posamentier, H.W., Van Wagoner, J.C. (Eds.), *Sea-level Changes: an Integrated Approach*. Society of Economic Paleontologists and Mineralogists, Tulsa, pp. 39–45.
- Vannier, F., Durand, J., 1994. Stratigraphie haute résolution d'un réservoir miocène du delta du Niger. *Bulletin des Centres de Recherches Exploration-Production Elf-Aquitaine* 18 (1), 1–18.

- Vendeville, B.C., 2005. Salt tectonics driven by sediment progradation: part I – mechanics and kinematics. *American Association of Petroleum Geologists Bulletin* 89 (8), 1071–1079.
- Vendeville, B.C., Cobbold, P.R., 1988. How normal faulting and sedimentation interact to produce listric fault profiles and stratigraphic wedges. *Journal of Structural Geology* 10, 649–659.
- Walsh, J.J., Nicol, A., Childs, C., 2002. An alternative model for the growth of faults. *Journal of Structural Geology* 24 (11), 1669–1675.
- Webb, H.F., Jordan, T.H., 2001. Pelagic sedimentation on rough seafloor topography 1. Forward Model. *Journal of Geophysical Research* 106 (B12), 30433–30449.
- White, N.J., Jackson, J.A., McKenzie, D.P., 1986. The relationship between the geometry of normal faults and that of the sedimentary layer in their hanging-walls. *Journal of Structural Geology* 8, 897–909.
- Whiteman, A., 1982. *Nigeria: its Petroleum Geology, Resources and Potential*, 1&2. Graham & Trotman, London, 394 pp.